Int J Adv Manuf Technol (2017) 93:2201–2214
DOI 10.1007/s00170-017-0692-4

ORIGINAL ARTICLE

High-order full-discretization methods for milling stability prediction by interpolating the delay term of time-delayed differential equations

Kai Zhou[1] · **Pingfa Feng**[1,2] · **Chao Xu**[1] · **Jianfu Zhang**[2] · **Zhijun Wu**[2]

Received: 23 March 2017 / Accepted: 14 June 2017 / Published online: 28 June 2017

Abstract The full-discretization method (FDM) has been proven effective for prediction on the regenerative chatter in many papers. However, the previous studies towards FDM just focused on high-order Lagrange interpolation for state term of time-delayed differential equations (DDEs), which formulates the dynamics model in milling process. It is well known that the discretization error caused by the delay term of DDEs would transmit to the state term inevitably; higher-order Lagrange interpolation for delay term is thus vital. In this paper, second-order, third-order, and fourth-order full-discretization methods using Lagrange interpolation for the delay term of DDEs (DFDMs) were firstly proposed. Then, influence on the accuracy, computational efficiency, and convergence rate of the proposed DFDMs was discussed in detail as the change of interpolation order. It was found that rise in accuracy and convergence rate of the proposed DFDM nearly stopped when the interpolation order for delay term was up to fourth order. Next, some researches on 2-degree-of-freedom (2-DOF) of dynamic system was studied and the results show that the proposed method using fourth-order Lagrange interpolation for the delay term of DDEs (4th DFDM) was effective. Finally, this paper verified the 4th DFDM by experiment and analyzed the prediction error of 4th DFDM, which may be caused by the modeling process of cutting force. The proposed DFDMs are developed to find a better method, which can update the existing FDM and make regenerative chatter's prediction more efficient and precise.

Keywords Milling · Machine tool dynamics · Chatter prediction · Full-discretization method

Highlights Stability prediction method based on interpolating DDEs' delay term was proposed.
High-order Lagrange interpolating for delay term was calculated to improve efficiency.
The proposed method proved to be more efficient and precise from numerical analysis.

✉ Chao Xu
xu.chao@sz.tsinghua.edu.cn

[1] Division of Advanced Manufacturing, Graduate School at Shenzhen, Tsinghua University, Shenzhen 518055, China

[2] Department Mechanical Engineering, Tsinghua University, Beijing 100084, China

1 Introduction

Chatter is a common phenomenon that can influence machining accuracy and efficiency of the machine tool in the milling, turning, and boring process. Therefore, chatter prediction is important to ensure the stability of machining process and to improve production efficiency by choosing optimal cutting parameter. In general, chatter phenomenon includes regenerative chatter, frictional chatter, and model coupling chatter. Among them, regenerative chatter is the most common form which has more effects on milling process. The prediction methods of regenerative chatter mainly include experimental method [1], analytical method and numerical method. The cost of experimental method is very high, and when conditions like material of workpiece and type of tool change, the previous stability lobe diagram will be no longer applicable, which is obtained by numerous cutting experiments. In summary, experimental method has disadvantages in the economy and adaptability. On the contrary, the analytical and numerical methods of regenerative chatter excel in the aspects of economy and adaptability. It can obtain the stability lobe diagram with high accuracy, only on the premise of acquiring modal parameters of milling spindle. The literature review of

analytical and numerical methods concerning regenerative chatter's prediction is given as follows.

Sridhar et al. [2] used linear differential equations to describe the dynamics model of milling and proposed a milling stability algorithm to predict the occurrence of milling chatter. Altinas et al. [3] proposed the zero-order analytical method (ZOA method), which analyzed the transfer function of the milling dynamics equation in the frequency domain and obtained the stability lobe diagram based on the mean of dynamic milling coefficients. This is the fastest method for predicting the occurrence of regenerative chatter, which is widely utilized. For example, Tang et al. [4] predicted regenerative chatter by using the ZOA method, considering the effects of multimode dynamics of the system at the same time. However, the ZOA method cannot predict the additional stability region that occurs when the radial depth of cut is small. Gradisek et al. [5] confirmed the above disadvantage of ZOA method by comparing ZOA method's prediction result with experimental results when the radial depth of cut was gradually decreased. In order to solve this problem and improve the accuracy of prediction, Budak et al. [6] improved the ZOA method and proposed a multi-frequency solution method which had good prediction accuracy in small radial cutting depth.

Many numerical methods for chatter's prediction has been put forward in recent years, including semi-discretization method (SDM) [7–10], numerical integration method [11, 12], full-discretization method (FDM) [13–18], Runge-Kutta-based discretization method [19], Euler-based discretization method [20], and so on. In summary, the difference between various existing numerical methods is mainly reflected in the mathematic method to deal with the dynamic model formulated by delayed differential equations (DDEs) in the process of numerical computation. Among the above numerical methods, SDM and FDM are more concerned and used by researchers.

The semi-discretization method is a numerical method and was proposed by Insperger et al. [7, 8]. Its main steps were to deform the milling dynamics equation into DDEs firstly. Then, the periodic and delay terms of DDEs is discretized by dividing the delay time into several parts; a series of ordinary differential equations (ODEs) are thus obtained. Next, the interpolation methods to periodic and delay terms, such as Lagrange interpolation, are used in the integral computation of ODEs. Finally, the transfer function of ODEs was obtained in the time domain and the stability of the transfer function was evaluated by Floquet theory to obtain the stability lobe diagram. Insperger et al. [7, 8] interpolated the period term of DDEs with piecewise function and interpolated the delay term with weight function based on the two ends of the interval; this method was called the 0th SDM. In order to make the SDM more efficient and accurate in the same divided parts of delay time, Insperger et al. [9] interpolated the delay term of DDEs with higher-order Lagrange interpolation. Gradisek et al. [5] found that the SDM can predict additional regenerative chatter that cannot be predicted by the ZOA method which occurs when the radial cutting depth is small. Ahmadi et al. [10] used the SDM to predict the regenerative chatter of the circular milling process. The prediction results are in good agreement with experimental results under different radial cutting depth.

Full-discretization method was proposed by Ding et al. [13]. This numerical method was in fact an extension of the SDM: it also discretized the state term of DDEs, together with the periodic and delay terms at the beginning, and thus realizing the complete discretization of DDEs. Accuracy of FDM was almost the same as that of SDM, but the computational efficiency was obviously improved. Ding et al. [13] performed a linear interpolation on the state term, periodic term, and delay term of DDEs, which was called 1st FDM. Just as mentioned above, different interpolation methods are used as follows to make the FDM more efficient and accurate in the same divided parts of delay time.

After putting forward the 1st FDM, Ding et al. [14] then performed second-order Lagrange interpolation on the state term of DDEs, which was called 2nd FDM. The 2nd FDM is found to have an obvious advantage over the 1st FDM in the aspects of convergence rate and prediction accuracy, but the computing time was only increased a little. Next, Quo et al. [15] approximated the state term of DDEs using third-order Lagrange interpolation. It was found that the convergence rate and prediction accuracy of 3rd FDM was higher than those of 1st FDM, 2nd FDM, and SDM. Ozoegwu et al. [16] studied the influence of the fourth- and fifth-order Lagrange interpolation for the state term on the accuracy and convergence rate of the FDM method, which was called 4th FDM and 5th FDM. They found that the accuracy of 4th FDM was the highest, and precision of the FDM was reduced when interpolating to fifth order for DDEs' state term. Ding et al. [13, 14], Guo et al. [15], and Ozoegwu et al. [16] studied the influence of Lagrange interpolation for DDEs' state term on the accuracy, computational efficiency, and convergence rate of FDM while the delay term was only approximated by using linear interpolation. Since the discrete error of the delay term can pass to the state term, higher-order interpolation for the delay term may be more efficient and accurate than that for state term. Therefore, some researchers approximated the delay term of DDEs, too. Liu et al. [17] performed second-order Lagrange interpolation for the delay term of the FDM and third-order Hermit interpolation for the state term at the same time. Tang et al. [18] performed second-order Lagrange interpolation on both the delay term and the state term of the FDM. It can be concluded that Liu et al. [17] and Tang et al. [18] only performed second-order interpolation on the delay term, and neither separately studied the effect of the interpolation order for the delay term on the prediction accuracy of the FDM.

Thus, this paper focuses on the effect of the delay term's interpolation order of the DDEs on the accuracy, convergence,

and computational efficiency of the proposed FDMs and makes detailed comparisons with the existing FDM and SDM to study the characteristics and advantages of developing the proposed FDMs.

To distinguish with the existing FDM interpolating for state term of DDEs, the proposed FDM using Lagrange interpolation for delay term is called DFDM. The proposed FDM with second-order, third-order, and fourth-order Lagrange interpolation for delay term are called 2nd DFDM, 3rd DFDM, and 4th DFDM respectively.

The rest of this paper is organized as follows. In Sect. 2, the mathematical model of DFDMs will be proposed with second-order, third-order, and fourth-order interpolation for delay term of DDEs respectively. In Sect. 3, the accuracy and computational efficiency of stability lobe diagrams obtained by DFDMs will be discussed, by comparing with the existing FDMs and the updated SDM. The discretization error of the proposed DFDMs is discussed in detail, and the change of 2-degree-of-freedom (2-DOF) stability lobe diagram using 4th DFDM when the radial immersion ratio a/D changes from 1 to 0.05 is analyzed. The difference of stability lobe diagrams between down-milling and up-milling is analyzed as well. In Sect. 4, experimental verification is presented to prove the accuracy of the proposed DFDMs, by using 4th DFDM. Section 5 concludes this paper.

2 The mathematical model of the proposed DFDM

2.1 The 1-DOF milling process

The dynamics equation of a 1-degree-of-freedom (1-DOF) milling tool with regenerative chatter can be expressed as literatures [8, 21]:

$$\ddot{x}(t) + 2\xi\omega_n\dot{x}(t) + {\omega_n}^2 x(t) = -\frac{wh(t)}{m_t}(x(t)-x(t-T)), \quad (1)$$

where ξ is the relative damping, ω_n is natural angular frequency, m_t is the modal mass of the tool, w is axial cutting depth, and the delay time T is equal to the tool passing period which is $60/(N\Omega)$ where N is the number of the cutter teeth and Ω is the spindle speed. $h(t)$ is the cutting force coefficient which is defined as

$$h(t) = \sum_{j=1}^{N} g\left(\phi_j(t)\right)\sin\left(\phi_j(t)\right)\left[K_t\cos\left(\phi_j(t)\right) + K_n\sin\left(\phi_j(t)\right)\right], \quad (2)$$

where K_t is the tangential cutting force coefficient and K_n the normal cutting force coefficient; $\phi_j(t)$ is the angular position of the jth tooth defined by

$$\phi_j(t) = (2\pi\,\Omega/60)t + (j-1)2\pi/N. \quad (3)$$

$g(\phi_j(t))$ is defined as

$$g\left(\phi_j(t)\right) = \begin{cases} 1 & if\ \phi_{st} < \phi_j(t) < \phi_{ex} \\ 0 & others \end{cases}. \quad (4)$$

where ϕ_{st},ϕ_{ex} are the start and exit angles of the jth cutter tooth, respectively. For down-milling,$\phi_{st} = \arccos(2a/D - 1)$,$\phi_{ex} = \pi$. For up-milling, $\phi_{st} = 0$,$\phi_{ex} = \arccos(1 - 2a/D)$, where a/D is the radial immersion ratio. The milling dynamics equation can be transformed into

$$\dot{\boldsymbol{z}}(t) = \boldsymbol{A}_0\boldsymbol{z}(t) + \boldsymbol{A}(t)\boldsymbol{z}(t) + \boldsymbol{B}(t)\boldsymbol{z}(t-T). \quad (5)$$

The terms in Eq. (5) are given in Eq. (32), which can be found in Appendix.

2.2 The 2-DOF milling process

For systems without coordinate coupling, the dynamics equation of a 2-DOF milling tool with regenerative chatter can be expressed as follows [8]:

$$\begin{bmatrix} m_t & 0 \\ 0 & m_t \end{bmatrix}\begin{bmatrix} \ddot{x}(t) \\ \ddot{y}(t) \end{bmatrix} + \begin{bmatrix} 2m_t\xi\omega_n & 0 \\ 0 & 2m_t\xi\omega_n \end{bmatrix}\begin{bmatrix} \dot{x}(t) \\ \dot{y}(t) \end{bmatrix} + \begin{bmatrix} {m_t\omega_n}^2 & 0 \\ 0 & {m_t\omega_n}^2 \end{bmatrix}\begin{bmatrix} x(t) \\ y(t) \end{bmatrix} = \begin{bmatrix} -wh_{xx}(t) & -wh_{xy}(t) \\ -wh_{yx}(t) & -wh_{yy}(t) \end{bmatrix}\begin{bmatrix} x(t) \\ y(t) \end{bmatrix} + \begin{bmatrix} wh_{xx}(t) & wh_{xy}(t) \\ wh_{yx}(t) & wh_{yy}(t) \end{bmatrix}\begin{bmatrix} x(t-T) \\ y(t-T) \end{bmatrix}, \quad (6)$$

where

$$\begin{aligned} h_{xx}(t) &= \sum_{j=1}^{N} g\left(\phi_j(t)\right)\sin\left(\phi_j(t)\right)\left[K_t\cos\left(\phi_j(t)\right) + K_n\sin\left(\phi_j(t)\right)\right], \\ h_{xy}(t) &= \sum_{j=1}^{N} g\left(\phi_j(t)\right)\cos\left(\phi_j(t)\right)\left[K_t\cos\left(\phi_j(t)\right) + K_n\sin\left(\phi_j(t)\right)\right], \\ h_{yx}(t) &= \sum_{j=1}^{N} g\left(\phi_j(t)\right)\sin\left(\phi_j(t)\right)\left[-K_t\sin\left(\phi_j(t)\right) + K_n\cos\left(\phi_j(t)\right)\right], \\ h_{yy}(t) &= \sum_{j=1}^{N} g\left(\phi_j(t)\right)\cos\left(\phi_j(t)\right)\left[-K_t\sin\left(\phi_j(t)\right) + K_n\cos\left(\phi_j(t)\right)\right]. \end{aligned} \quad (7)$$

The milling dynamics equation can be transformed into

$$\dot{\boldsymbol{z}}(t) = \boldsymbol{A}_0\boldsymbol{z}(t) + \boldsymbol{A}(t)\boldsymbol{z}(t) + \boldsymbol{B}(t)\boldsymbol{z}(t-T). \quad (8)$$

The terms in Eq. (8) are given in Eq. (34) in Appendix.

2.3 The proposed mathematical model based on DDEs

As is seen from the above expressions, the dynamics equation of both 1-DOF milling process and 2-DOF milling process can be described by DDEs, which can be expressed as

$$\dot{z}(t) = \boldsymbol{A}_0 \boldsymbol{z}(t) + \boldsymbol{A}(t)\boldsymbol{z}(t) + \boldsymbol{B}(t)\boldsymbol{z}(t-T). \tag{9}$$

where $\boldsymbol{A}_0$ is a constant matrix which is decided by the milling system parameters, and $\boldsymbol{A}(t)$ and $\boldsymbol{B}(t)$ are two periodic matrices satisfying $\boldsymbol{A}(t) = \boldsymbol{A}(t+T)$ and $\boldsymbol{B}(t) = \boldsymbol{B}(t+T)$ where T is the delay time. The delay time T of the above equation is equidistantly divided into m parts, which is $T = m\tau$; the above equation can be deformed into the following equation in $[k\tau, k\tau+\tau]$:

$$\boldsymbol{z}(t) = \mathrm{e}^{\boldsymbol{A}_0(t-k\tau)}\boldsymbol{z}(k\tau) + \int_{k\tau}^{t} \left\{ \mathrm{e}^{\boldsymbol{A}_0(t-\xi)}[\boldsymbol{A}(\xi)\boldsymbol{z}(\xi) + \boldsymbol{B}(\xi)\boldsymbol{z}(\xi-T)] \right\} d\xi. \tag{10}$$

where $t \in [k\tau, k\tau+\tau]$.

Eq. (10) can be equivalently expressed as

$$\begin{aligned} \boldsymbol{z}_{k+1} = \mathrm{e}^{\boldsymbol{A}_0\tau}\boldsymbol{z}_k + \int_0^{\tau} \{ & \mathrm{e}^{\boldsymbol{A}_0\xi}[\boldsymbol{A}(k\tau+\tau-\xi)\boldsymbol{z}(k\tau+\tau-\xi) \\ & + \boldsymbol{B}(k\tau+\tau-\xi)\boldsymbol{z}(k\tau+\tau-\xi-T)] \} d\xi \end{aligned} \tag{11}$$

where $\boldsymbol{z}(k\tau)$ is expressed by $\boldsymbol{z}_k$.

In order to facilitate the integral calculation, periodic term, delay term, and state term of Eq. (11) are discretized and interpolated as follows:

$$\begin{aligned} \boldsymbol{z}(k\tau+\tau-\xi) &= \boldsymbol{z}_{k+1} + \xi(\boldsymbol{z}_k - \boldsymbol{z}_{k+1})/\tau \\ \boldsymbol{A}(k\tau+\tau-\xi) &= \boldsymbol{A}_{k+1} + \xi(\boldsymbol{A}_k - \boldsymbol{A}_{k+1})/\tau \\ \boldsymbol{B}(k\tau+\tau-\xi) &= \boldsymbol{B}_{k+1} + \xi(\boldsymbol{B}_k - \boldsymbol{B}_{k+1})/\tau \end{aligned} \tag{12}$$

The purpose of this paper is to perform higher-order Lagrange interpolation on the delay terms, so the state and period terms of the DDEs above are simply performed with linear Lagrange interpolation.

The description of the periodic term is simplified as

$$\begin{aligned} \boldsymbol{A}(k\tau+\tau-\xi) &= \boldsymbol{A}_0{}^{(k)} + \boldsymbol{A}_1{}^{(k)}\xi, \\ \boldsymbol{B}(k\tau+\tau-\xi) &= \boldsymbol{B}_0{}^{(k)} + \boldsymbol{B}_1{}^{(k)}\xi, \end{aligned} \tag{13}$$

where

$$\begin{aligned} \boldsymbol{A}_0{}^{(k)} &= \boldsymbol{A}_{k+1}, \\ \boldsymbol{A}_1{}^{(k)} &= (\boldsymbol{A}_k - \boldsymbol{A}_{k+1})/\tau, \\ \boldsymbol{B}_0{}^{(k)} &= \boldsymbol{B}_{k+1}, \\ \boldsymbol{B}_1{}^{(k)} &= (\boldsymbol{B}_k - \boldsymbol{B}_{k+1})/\tau \end{aligned} \tag{14}$$

*P*th-order Lagrange interpolation for delay term of DDEs uses the following elements:

$$\boldsymbol{z}_{k-m}, \boldsymbol{z}_{k-m+1}, \boldsymbol{z}_{k-m+2} \cdots \boldsymbol{z}_{k-m+p}.$$

The expression is

$$\begin{aligned} & \boldsymbol{z}((k-m+1)\tau\text{-}\xi) \\ & = \sum_{\substack{l=0 \\ l\neq\lambda}}^{p} \frac{((k-m+l)\tau-\xi-(k-m)\tau)((k-m+l)\tau-\xi-(k-m+1)\tau)\cdots}{((k-m+l)\tau-(k-m)\tau)((k-m+l)\tau-(k-m+1)\tau)\cdots} \\ & \quad \frac{\cdots((k-m+l)\tau-\xi-(k-m+\lambda)\tau)\cdots((k-m+l)\tau-\xi-(k-m+p)\tau)}{\cdots((k-m+l)\tau-(k-m+\lambda)\tau)\cdots((k-m+l)\tau-(k-m+p)\tau)} \boldsymbol{z}_{k-m+l} \end{aligned} \tag{15}$$

In order to study the influence of the delay term's order on the prediction's accuracy, computational efficiency, and convergence rate, second-order, third-order, and fourth-order Lagrange interpolation for delay term are done as follows. Sections 2.3.1, 2.3.2, and 2.3.3 are the primary mathematical derivation processes of 2nd DFDM, 3rd DFDM, and 4th DFDM respectively.

2.3.1 When the order of Lagrange interpolation is p = 2

The delay term $\boldsymbol{z}(k\tau+\tau-\xi-T)$ is approximated by second-order Lagrange interpolation, which is as follows

$$\boldsymbol{z}(k\tau+\tau-\xi-T) = \frac{\xi^2+\tau\xi}{2\tau^2}\boldsymbol{z}_{k-m} + \frac{-\xi^2+\tau^2}{\tau^2}\boldsymbol{z}_{k-m+1} + \frac{\xi^2-\tau\xi}{2\tau^2}\boldsymbol{z}_{k-m+2}. \tag{16}$$

Substituting Eqs. (16) and (12) into Eq. (11), Eq. (17) can be obtained as follows:

$$\begin{aligned} \boldsymbol{z}_{k+1} = & (\boldsymbol{F}_0 + \boldsymbol{F}_k)\boldsymbol{z}_k + \boldsymbol{F}_{k+1}\boldsymbol{z}_{k+1} + \boldsymbol{F}_m\boldsymbol{z}_{k-m} \\ & + \boldsymbol{F}_{m+1}\boldsymbol{z}_{k-m+1} + \boldsymbol{F}_{m+2}\boldsymbol{z}_{k-m+2}. \end{aligned} \tag{17}$$

The terms in Eq. (17) are given in Eq. (36) in Appendix.

Ding et al. [13] has proved that $(\boldsymbol{I}\text{-}\boldsymbol{F}_{k+1})$ is non-singular. Hence, $\boldsymbol{z}_{k+1}$ can be expressed in the following explicit equation:

$$\begin{aligned} \boldsymbol{z}_{k+1} = & (\boldsymbol{I}-\boldsymbol{F}_{k+1})^{-1}(\boldsymbol{F}_0 + \boldsymbol{F}_k)\boldsymbol{z}_k + (\boldsymbol{I}-\boldsymbol{F}_{k+1})^{-1}\boldsymbol{F}_m\boldsymbol{z}_{k\text{-}m} \\ & + (\boldsymbol{I}-\boldsymbol{F}_{k+1})^{-1}\boldsymbol{F}_{m+1}\boldsymbol{z}_{k-m+1} + (\boldsymbol{I}-\boldsymbol{F}_{k+1})^{-1}\boldsymbol{F}_{m+2}\boldsymbol{z}_{k-m+2}. \end{aligned} \tag{18}$$

The submatrix $\boldsymbol{D}_k$ is defined as

$$\boldsymbol{V}_{k+1} = \boldsymbol{D}_k\boldsymbol{V}_k, \tag{19}$$

where

$$\boldsymbol{V}_k = (\boldsymbol{z}_k, \boldsymbol{z}_{k\text{-}1}, \boldsymbol{z}_{k\text{-}2}, \cdots, \boldsymbol{z}_{k\text{-}m})^{\mathrm{T}}. \tag{20}$$

Eq. (21) can be obtained according to Eqs. (19) and (20):

$$\boldsymbol{D}_k = \begin{bmatrix} (\boldsymbol{I}-\boldsymbol{F}_{k+1})^{-1}(\boldsymbol{F}_0+\boldsymbol{F}_k)\cdots(\boldsymbol{I}-\boldsymbol{F}_{k+1})^{-1}\boldsymbol{F}_{m+2} & (\boldsymbol{I}-\boldsymbol{F}_{k+1})^{-1}\boldsymbol{F}_{m+1} & (\boldsymbol{I}-\boldsymbol{F}_{k+1})^{-1}\boldsymbol{F}_m \\ \boldsymbol{I} & & \\ & \boldsymbol{I} & \\ & & \boldsymbol{I} \\ & & & \boldsymbol{I} \\ & & & & \boldsymbol{I} \\ & & & & & \boldsymbol{I} \\ & & & & & & \boldsymbol{I} \end{bmatrix} \tag{21}$$

The transition matrix $\boldsymbol{\Phi}$ is defined as

$$\boldsymbol{V}_m = \boldsymbol{\Phi}\boldsymbol{V}_0, \tag{22}$$

where

$$\boldsymbol{\Phi} = \boldsymbol{D}_{m-1}\boldsymbol{D}_{m-2}\cdots\boldsymbol{D}_1\boldsymbol{D}_0. \tag{23}$$

According to the Floquet theory [7, 22], if all the eigenvalues of the transition matrix $\boldsymbol{\Phi}$ are in modulus less than 1, the system can be considered to be stable and no regenerative chatter will occur. Otherwise, it is unstable.

2.3.2 When the order of Lagrange interpolation is $p = 3$

The delay term $z(k\tau+\tau-\xi-T)$ is approximated by third-order Lagrange interpolation, which is as follows:

$$z(k\tau+\tau-\xi-T) = \frac{\xi^3+3\tau\xi^2+2\tau^2\xi}{6\tau^3}\boldsymbol{z}_{k-m} + \frac{-\xi^3-2\tau\xi^2+\tau^2\xi+2\tau^3}{2\tau^3}\boldsymbol{z}_{k-m+1} + \frac{\xi^3+\tau\xi^2-2\tau^2\xi}{2\tau^3}\boldsymbol{z}_{k-m+2} + \frac{-\xi^3+\tau^2\xi}{6\tau^3}\boldsymbol{z}_{k-m+3} \tag{24}$$

Substituting Eqs. (24) and (12) into Eq. (11), Eq. (25) can be obtained as follows:

$$\boldsymbol{z}_{k+1} = (\boldsymbol{F}_0+\boldsymbol{F}_k)\boldsymbol{z}_k + \boldsymbol{F}_{k+1}\boldsymbol{z}_{k+1} + \boldsymbol{F}_m\boldsymbol{z}_{k-m} + \boldsymbol{F}_{m+1}\boldsymbol{z}_{k-m+1} + \boldsymbol{F}_{m+2}\boldsymbol{z}_{k-m+2} + \boldsymbol{F}_{m+3}\boldsymbol{z}_{k-m+3} \tag{25}$$

The terms in Eq. (25) are given in Eq. (38) in Appendix. $\boldsymbol{z}_{k+1}$ can be expressed in the following explicit form:

$$\boldsymbol{z}_{k+1} = (\boldsymbol{I}-\boldsymbol{F}_{k+1})^{-1}(\boldsymbol{F}_0+\boldsymbol{F}_k)\boldsymbol{z}_k + (\boldsymbol{I}-\boldsymbol{F}_{k+1})^{-1}\boldsymbol{F}_m\boldsymbol{z}_{k-m} + (\boldsymbol{I}-\boldsymbol{F}_{k+1})^{-1}\boldsymbol{F}_{m+1}\boldsymbol{z}_{k-m+1} + (\boldsymbol{I}-\boldsymbol{F}_{k+1})^{-1}\boldsymbol{F}_{m+2}\boldsymbol{z}_{k-m+2} + (\boldsymbol{I}-\boldsymbol{F}_{k+1})^{-1}\boldsymbol{F}_{m+3}\boldsymbol{z}_{k-m+3} \tag{26}$$

The submatrix $\boldsymbol{D}_k$ can be obtained using the same method mentioned in Sect. 2.3.1:

$$\boldsymbol{D}_k = \begin{bmatrix} (\boldsymbol{I}-\boldsymbol{F}_{k+1})^{-1}(\boldsymbol{F}_0+\boldsymbol{F}_k)\cdots(\boldsymbol{I}-\boldsymbol{F}_{k+1})^{-1}\boldsymbol{F}_{m+3} & (\boldsymbol{I}-\boldsymbol{F}_{k+1})^{-1}\boldsymbol{F}_{m+2} & (\boldsymbol{I}-\boldsymbol{F}_{k+1})^{-1}\boldsymbol{F}_{m+1} & (\boldsymbol{I}-\boldsymbol{F}_{k+1})^{-1}\boldsymbol{F}_m \\ \boldsymbol{I} & & & \\ & \boldsymbol{I} & & \\ & & \boldsymbol{I} & \\ & & & \boldsymbol{I} \\ & & & & \boldsymbol{I} \\ & & & & & \boldsymbol{I} \\ & & & & & & \boldsymbol{I} \end{bmatrix} \tag{27}$$

The transition matrix $\boldsymbol{\Phi}$ can also be obtained in the same way mentioned in Sect. 2.3.1.

2.3.3 When the order of Lagrange interpolation is $p = 4$

The delay term $\boldsymbol{z}(k\tau+\tau-\xi-T)$ is approximated by fourth-order Lagrange interpolation, which is as follows:

$$z(k\tau+\tau-\xi-T) = \frac{\xi^4+6\tau\xi^3+11\tau^2\xi^2+6\tau^3\xi}{24\tau^4}\boldsymbol{z}_{k-m} + \frac{-\xi^4+5\tau\xi^3-5\tau^2\xi^2+5\tau^3\xi+6\tau^4}{6\tau^4}\boldsymbol{z}_{k-m+1} + \frac{\xi^4+4\tau\xi^3+\tau^2\xi^2-6\tau^3\xi}{4\tau^4}\boldsymbol{z}_{k-m+2} + \frac{-\xi^4-3\tau\xi^3+\tau^2\xi^2+3\tau^3\xi}{6\tau^4}\boldsymbol{z}_{k-m+3} + \frac{\xi^4+2\tau\xi^3-\tau^2\xi^2-2\tau^3\xi}{24\tau^4}\boldsymbol{z}_{k-m+4}. \tag{28}$$

Substituting Eqs. (28) and (12) into Eq. (11), Eq. (29) can be obtained as follows:

$$\begin{aligned} \boldsymbol{z}_{k+1} = (\boldsymbol{F}_0 + \boldsymbol{F}_k)\boldsymbol{z}_k + \boldsymbol{F}_{k+1}\boldsymbol{z}_{k+1} + \boldsymbol{F}_m\boldsymbol{z}_{k-m} + \boldsymbol{F}_{m+1}\boldsymbol{z}_{k-m+1} \\ + \boldsymbol{F}_{m+2}\boldsymbol{z}_{k-m+2} + \boldsymbol{F}_{m+3}\boldsymbol{z}_{k-m+3} + \boldsymbol{F}_{m+4}\boldsymbol{z}_{k-m+4} \end{aligned} \tag{29}$$

The terms in Eq. (29) are given in Eq. (40) in Appendix.

$\boldsymbol{z}_{k+1}$ can be expressed in the following explicit form:

$$\begin{aligned} \boldsymbol{z}_{k+1} = (\boldsymbol{I}-\boldsymbol{F}_{k+1})^{-1}(\boldsymbol{F}_0 + \boldsymbol{F}_k)\boldsymbol{z}_k + (\boldsymbol{I}-\boldsymbol{F}_{k+1})^{-1}\boldsymbol{F}_m\boldsymbol{z}_{k-m} \\ + (\boldsymbol{I}-\boldsymbol{F}_{k+1})^{-1}\boldsymbol{F}_{m+1}\boldsymbol{z}_{k-m+1} + (\boldsymbol{I}-\boldsymbol{F}_{k+1})^{-1}\boldsymbol{F}_{m+2}\boldsymbol{z}_{k-m+2} \\ + (\boldsymbol{I}-\boldsymbol{F}_{k+1})^{-1}\boldsymbol{F}_{m+3}\boldsymbol{z}_{k-m+3} + (\boldsymbol{I}-\boldsymbol{F}_{k+1})^{-1}\boldsymbol{F}_{m+4}\boldsymbol{z}_{k-m+4} \end{aligned} \tag{30}$$

The submatrix $\boldsymbol{D}_k$ can be obtained using the same method mentioned in Sect. 2.3.1

$$\boldsymbol{D}_k = \begin{bmatrix} (\boldsymbol{I}\text{-}\boldsymbol{F}_{k+1})^{-1}(\boldsymbol{F}_0 + \boldsymbol{F}_k)\cdots(\boldsymbol{I}-\boldsymbol{F}_{k+1})^{-1}\boldsymbol{F}_{m+4} & (\boldsymbol{I}-\boldsymbol{F}_{k+1})^{-1}\boldsymbol{F}_{m+3} & (\boldsymbol{I}-\boldsymbol{F}_{k+1})^{-1}\boldsymbol{F}_{m+2} & (\boldsymbol{I}-\boldsymbol{F}_{k+1})^{-1}\boldsymbol{F}_{m+1} & (\boldsymbol{I}-\boldsymbol{F}_{k+1})^{-1}\boldsymbol{F}_m \\ \boldsymbol{I} & & & & \\ & \boldsymbol{I} & & & \\ & & \boldsymbol{I} & & \\ & & & \boldsymbol{I} & \\ & & & & \boldsymbol{I} \end{bmatrix} \tag{31}$$

The transition matrix $\boldsymbol{\Phi}$ can also be obtained in the same way mentioned in Sect. 2.3.1.

3 Numerical stability computation results and discretization error analysis

In order to verify the proposed DFDMs and discover the characteristics and advantages of developing DFDMs, benchmark examples [8, 14, 15] are utilized in this section. The accuracy, computational efficiency, and convergence rate of DFDMs, corresponding to model of 1-DOF down-milling system, are illustrated and compared with the existing FDM and the SDM. In addition, the change of 2-DOF stability lobe diagram is discussed by using 4th DFDM, when the radial immersion ratio a/D changes from 1 to 0.05. The difference of stability lobe diagrams between down-milling and up-milling is discussed, as well. All the computer programs are written in MATLAB 2015b, and the programs' running environment is Inter(R) Core(TM) i3-4170CPU @3.70GHz 3.70 GHz RAM 8GB.

Table 1 Milling system parameters

The number of cutter teeth N	2	
The natural frequency ω_n	5793	rad/s
Relative damping ξ	0.011	
Modal mass m_t	0.03993	kg
The tangential cutting force coefficient K_t	6×10^8	N/m^2
The normal cutting force coefficient K_n	2×10^8	N/m^2

3.1 Stability lobe diagrams

In order to illustrate the accuracy of DFDMs, including 2nd DFDM, 3rd DFDM, and 4th DFDM, the stability lobe diagrams are shown in Table 2.

To make comparisons, Table 2 also lists the 1st FDM method proposed by Ding et al. [13], the 2nd FDM method proposed by Ding et al. [14], the 3rd FDM method proposed by Quo et al. [15], the 4th FDM method proposed by Ozoegwu et al. [16], and the SDM method proposed by Insperger et al. [8], recorded as updated SDM. The stability lobe diagrams are calculated over 200 × 100-sized grid of parameters with the boundaries of the rotational speed $\Omega \in [5.0 \times 10^3,\ 1.0 \times 10^4]$ rpm and axial cutting depth $w \in [0, 4 \times 10^{-3}]$ m. Table 1 is the milling system's parameters. Because of the instability of programs' running time using MATLAB, every program is run for three times to acquire the average running time. The average time-consuming value of the corresponding method is recorded in Table 2.

Table 2 lists the stability lobe diagrams and corresponding calculation time of MATLAB programs. The expression of each row in Table 2 was labeled, corresponding to eight kinds of methods. In addition, there are three columns in Table 2, corresponding to different discrete points of delay time T. Since the discretization error decreases by the discrete points m-value, the red line in Table 2 which is derived from the 1st

Table 2 Stability lobe diagrams obtained with different methods and different number of time intervals

	m=20	m=30	m=40
1	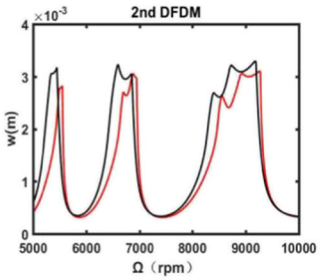	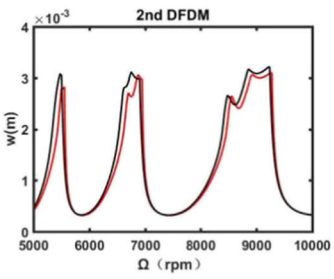	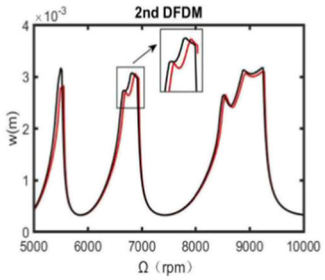
	20.51s	36.64s	61.89s
2	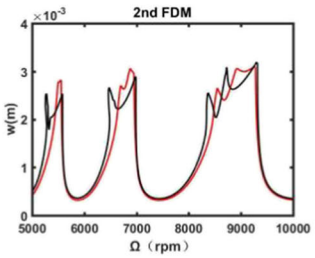	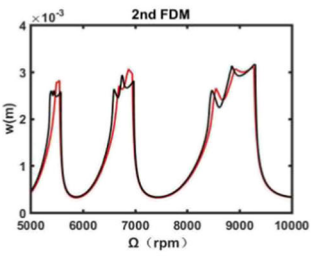	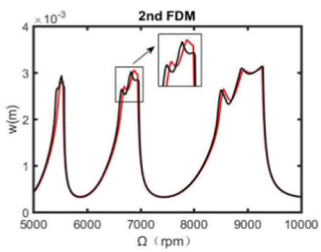
	20.81s	37.37s	63.22s
3	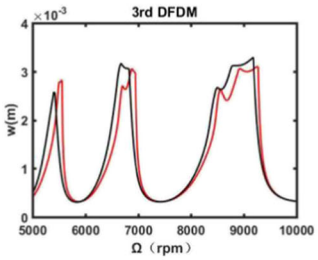	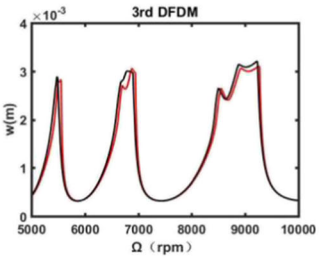	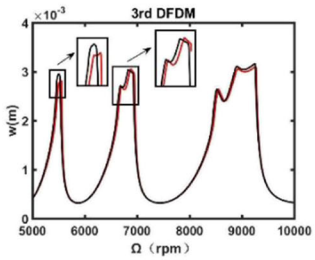
	22.80s	40.82s	67.65s
4	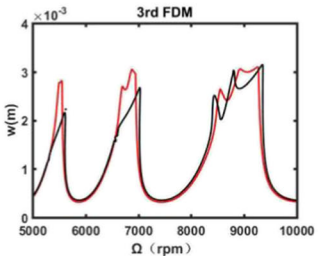	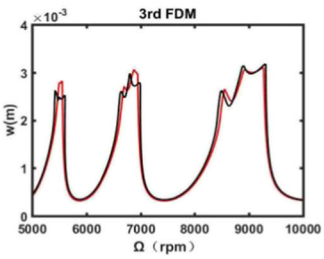	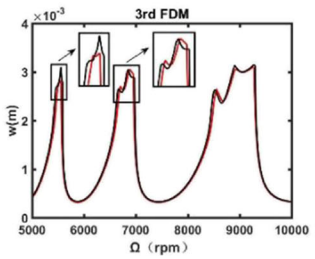
	23.31s	40.88s	67.39s

FDM method with m = 200 can be used as the ideal stability lobe diagrams to evaluate the accuracy of various methods.

Firstly, from the stability lobe diagrams of first, third, and fifth rows, we can make the following three conclusions:

1. The higher the order of delay term's Lagrange interpolation is, the more rapidly close the proposed method is to the ideal stability lobe diagram, with the increase of number of time interval m-value.
2. There is no apparent improvement in time cost when the order of delay term's Lagrange interpolation is higher.
3. The 4th DFDM has already good prediction accuracy when the m-value is up to 40; hence, it can be predicted reasonably that hyper-fourth-order DFDM cannot improve the accuracy of stability lobe diagram apparently compared with the fourth-order DFDM when the m-value is 40.

The above conclusions indicate that high-order DFDM can be taken as an alternative for precisely predicting stability lobe diagram with a small number of time interval m-value.

Table 2 (continued)

5	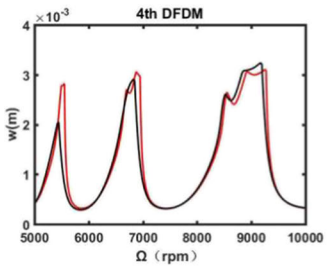	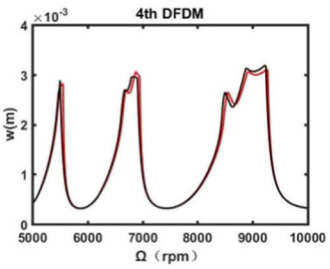	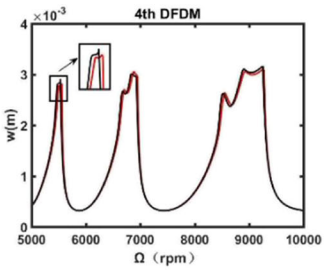
	25.92s	44.96s	73.63s
6	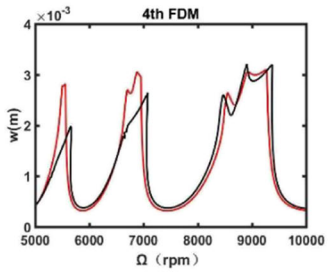	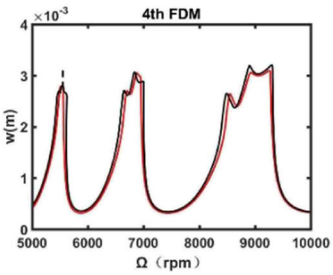	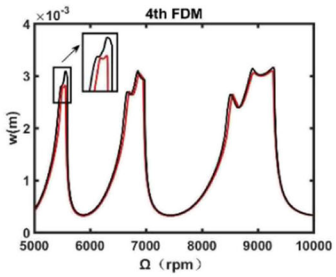
	26.17s	44.16s	75.88s
7	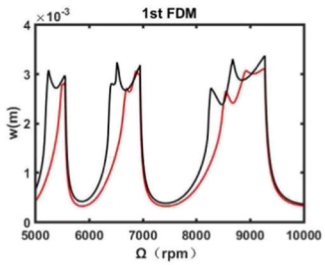	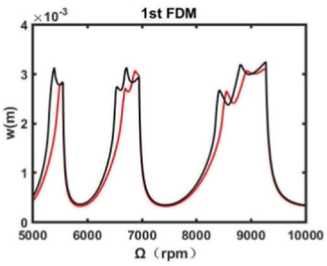	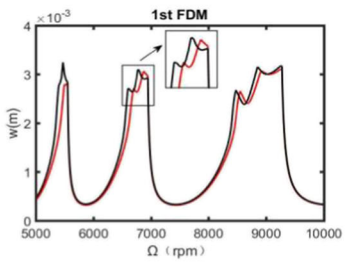
	16.2s	30.46s	55.57s
8	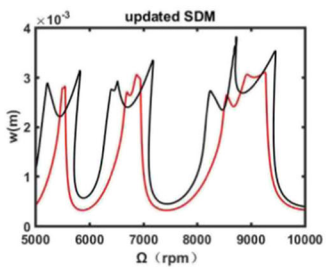	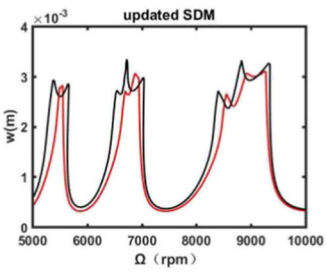	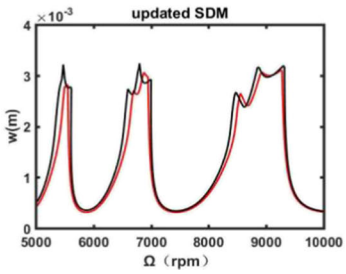
	79.51s	117.80s	189.43s

Then, compared with the updated SDM in the eighth row, the 2nd DFDM, 3rd DFDM, and 4th DFDM can obviously improve the accuracy and computational efficiency of the regenerative chatter prediction at the same m-value. DFDMs' prediction accuracy rises but computational efficiency declines, comparing with 1st FDM in the seventh row.

The above conclusion indicates that DFDMs are feasible and can be taken as an alternative for precisely predicting stability lobe diagrams with a small number of time interval m-value.

Finally, we can conclude from the comparison between the fifth and sixth rows that 4th DFDM is more rapidly close to the ideal stability lobe diagrams than 4th FDM, and the computation time of 4th DFDM is as a whole decreased in the meantime. From the comparison between the third and fourth rows in Table 2, we can draw conclusions that the computational efficiency of 3rd DFDM is slightly improved, on the

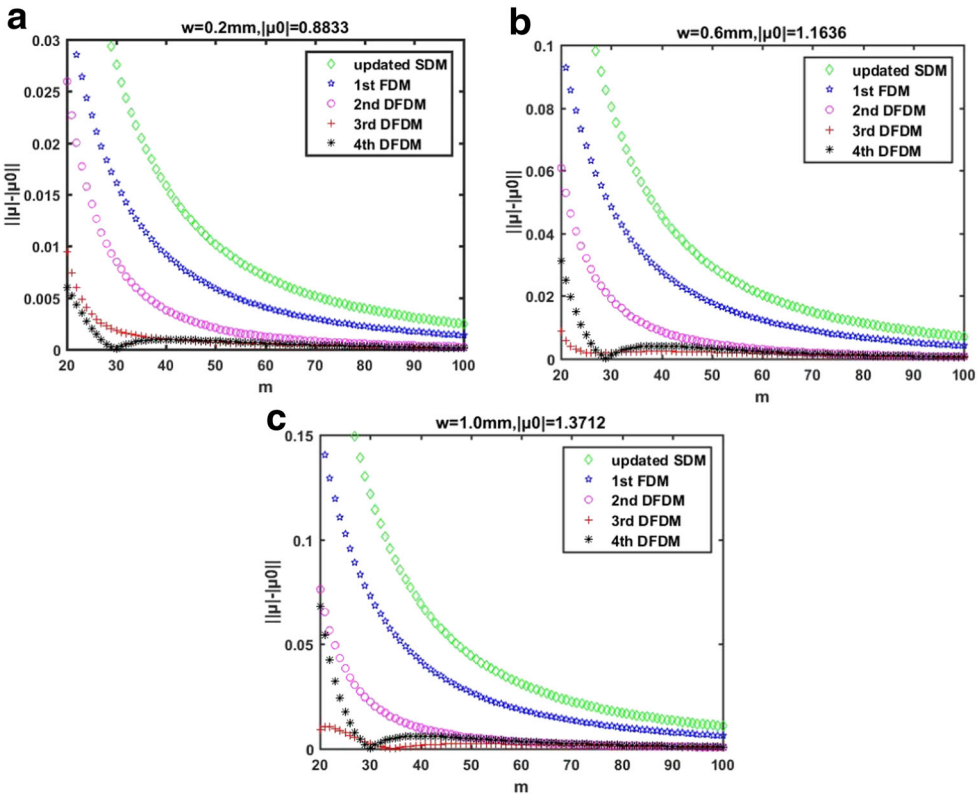

Fig. 1 Convergence of the eigenvalues for different number of time-intervals m for different methods. **a** The axial depth of cut $w = 0.2$ mm. **b** The axial depth of cut $w = 0.6$ mm. **c** The axial depth of cut $w = 1.0$ mm

whole, with the increase of number of time interval m-value, though 3rd FDM needs less computational time for m = 40. However, it is not apparent which is more rapidly close to the ideal stability lobe diagrams between 3rd FDM and 3rd DFDM.

Comparing the first with the second rows in Table 2, it is also not apparent which is more rapidly close to the ideal stability lobe diagrams between 2nd FDM and 2nd DFDM; however, the computation time of 2nd DFDM is slightly decreased. Hence, computational efficiency of 2nd DFDM is slightly improved.

The above conclusions indicate that Lagrange interpolation for delay term of DDEs is more efficient and precise than that for state term.

3.2 Convergence rate

Insperger et al. [9, 23] proposed a method of approximating discretization error, which involves comparing Taylor series solution and convolution integral over a discrete interval, to demonstrate that the local error of 0th SDM is $E_{0\text{th - SDM}} = O(\Delta t^2)$ and first-order FDM is $E_{1\text{st - FDM}} = O(\Delta t^2)$. Through the use of the same method, the following conclusions were obtained: 2nd FDM's discrete error is $E_{2\text{nd - FDM}} = O(\Delta t^3)$ [14], 3rd FDM's discrete error is $E_{3\text{rd - FDM}} = O(\Delta t^4)$ [15], and 4th FDM's discrete error is $E_{4\text{th - FDM}} = O(\Delta t^5)$ [16]. Using the same method, the 2nd, 3rd, and 4th DFDM's discrete error can be obtained as $E_{2\text{nd - DFDM}} = O(\Delta t^3)$, $E_{3\text{rd - DFDM}} = O(\Delta t^4)$, and $E_{4\text{th - DFDM}} = O(\Delta t^5)$.

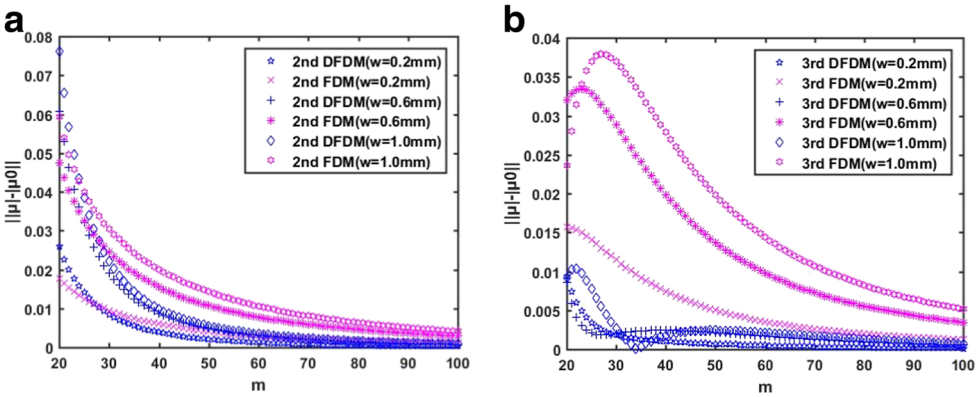

Fig. 2 Comparisons of eigenvalues' convergence of the DFDM and the existing FDM with different axial depths of cut *w*. **a** 2nd DFDM and 2nd FDM. **b** 3rd DFDM and 3rd FDM

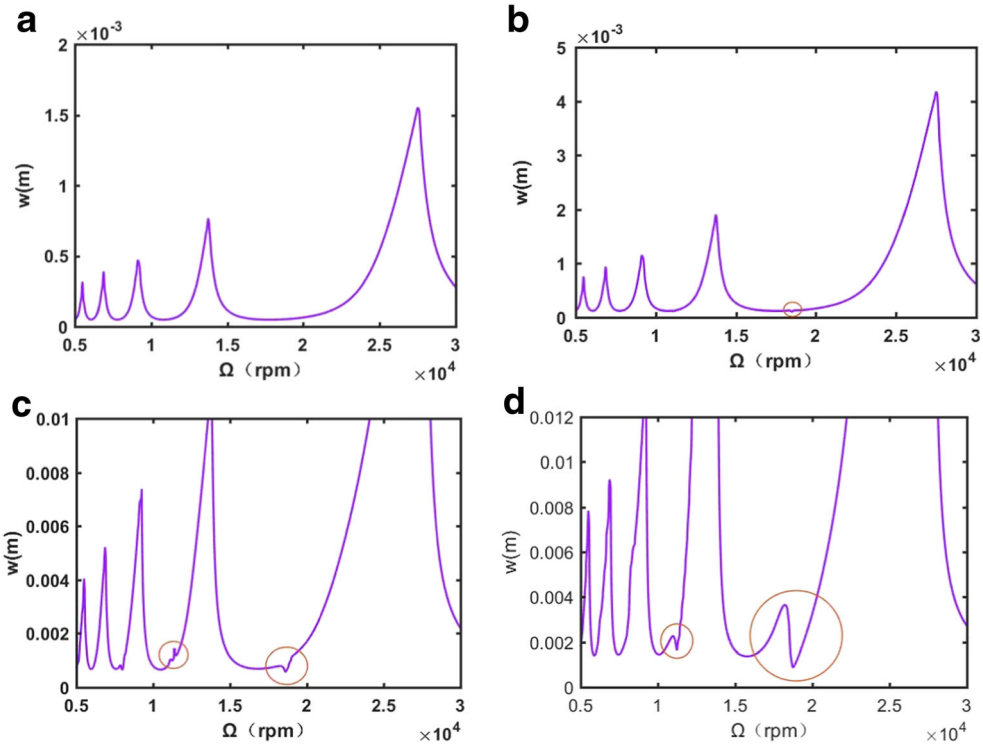

Fig. 3 The stability lobe diagrams of 2-DOF milling process with different radial immersion ratio a/D. **a** a/D = 1. **b** a/D = 0.5. **c** a/D = 0.1. **d** a/D = 0.05

In order to better illustrate the convergence of DFDMs, the absolute value of critical eigenvalue $|\mu|$ and the exact one $|\mu_0|$ are presented as the function of the computational parameter m, in Fig. 1, where $|\mu_0|$ is determined by using the method of updated SDM with m = 400. The spindle speed is 6000 rpm and the axial depth of cut is w = 0.2, 0.6, and 1.0 mm, respectively.

As shown in Fig. 1, with the increase of interpolation order of delay term, the difference decreases gradually in the same m-value. When the interpolation order of DFDM reaches fourth order, the influence of interpolation order on convergence rate can be neglected. Fourth DFDM can be regarded as the method with the fastest convergence rate in this case. In addition, compared with the updated SDM and 1st FDM, the proposed DFDMs have an obvious advantage in terms of the convergence rate.

As is show in Fig. 2, there are two comparisons concerning the convergence rate of $||\mu| - |\mu_0||$. It is concluded from Fig. 2a that 2nd DFDM's convergence rate is slightly faster than that of 2nd FDM. As can be seen from Fig. 2b, 3rd DFDM's convergence rate is faster than that of 3rd FDM obviously. According to the above comparisons, conclusions can be made that the DFDM has an advantage over the existing FDM in terms of the convergence rate.

3.3 2-DOF stability lobe diagram

From the analysis above, we can conclude that only the characteristics of 1-DOF milling system are studied. Nevertheless, from Sect. 2, the proposed DFDMs can be extended to a 2-DOF system. To analyze the proposed DFDMs better and more comprehensive, some researches on 2-DOF milling process are also made in the following.

Since 4th DFDM gives a stability diagram with m = 40 that coincides with the ideal stability lobe diagram better, 4th DFDM is used in this part for 2-DOF milling system. It can be observed from Fig. 3 that the stability limit gradually increases with the decrease of the radial immersion ratio a/D. At the same time, the additional stability region is gradually emerging, which has been circled. Quo et al. [15] and Ozoegwu et al. [16] have the similar conclusion. The existence of this region has been proved by experiments [5]. This is the advantage of SDM, existing FDM, and DFDM. It can predict the additional form of regenerative chatter which traditional prediction methods, such as ZOA method, cannot predict.

Figure 4 shows the comparison between down-milling and up-milling with 4th DFDM method when a/D = 0.5 and m = 40. As shown in Fig. 4, some conclusions can be made: (1) the stability limit of down-milling is slightly lower comparing with up-milling. This conclusion is based on the hypothesis that the workpiece is rigid. (2) The additional stability lobe diagrams of up-milling and down-milling appear almost at the same speed range and nearly have the same shape, which are affected slightly by the milling method.

Remark The difference of stability lobe diagrams between up-milling and down-milling should result from the loss-of-

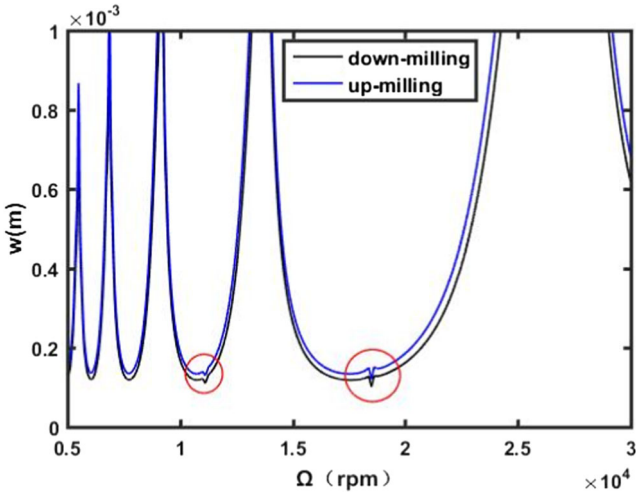

Fig. 4 Comparison of down-milling and up-milling with 4th DFDM

contact effect, which has been confirmed by Zhao et al. [24] and Long et al. [25]. In addition, the difference between up-milling and down-milling will be more prominent when the radial immersion ratio is reduced [24].

4 Experimental verification

Gradišek et al. [5] and Ahmadi et al. [10] proved the superiority of SDM through experiments, indirectly verifying the FDM. Yue et al. [26] verified 1st FDM with an improved cutting force model, by experiments. As a whole, experimental verification to FDM (including the proposed method: DFDM) is lacking. In this paper, the above-mentioned 4th DFDM corresponding to 2-DOF milling system with $m = 40$ is used, for example, to predict the regenerative chatter. System parameters and cutting experiment data come from Gradišek et al. [5]. Prediction result and experimental results are shown in Fig. 5.

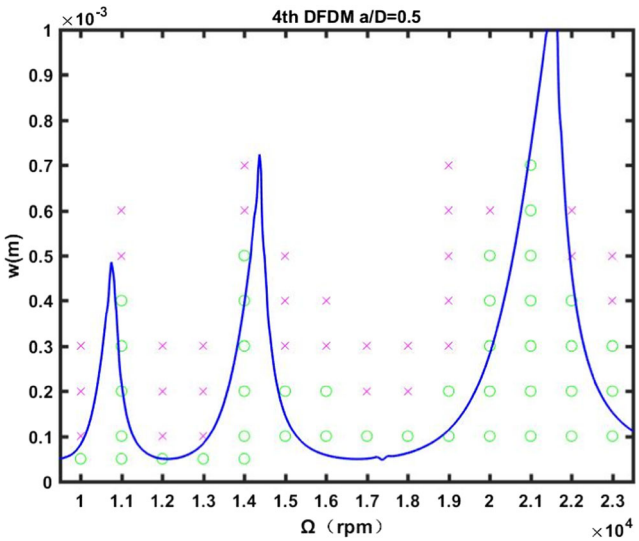

Fig. 5 Experimental and predicted stability boundaries for up-milling with a/D = 0.5, $m = 40$. Circles-stable cutting, crosses-chatter; *blue line*—4th DFDM's prediction

It can be seen from Fig. 5 that 4th DFDM can approximately predict the occurrence of the regenerative chatter when the radial immersion ratio a/D is 0.5. But in some speed range, for example, in the range of about 16,000 rpm and about 20,000 rpm, the error of prediction is relatively large.

Remark Some papers have mentioned that non-linearities of cutting force have an influence on the chatter's prediction and the study on the nature of chatter. These non-linearities include multiple regenerative effects, loss-of-contact effect, feed rate effect, and so on [27–29]. In addition, the process damping also has a depressant effect on the chatter's prediction and study on the nature of chatter. In recent years, many researchers have studied the process damping when modeling the cutting force [30–35]. What is more, the stiffness of the workpiece may have an impact on the chatter's prediction and study on the nature of chatter, which has been studied by many researchers [36, 37].

The nature of chatter can be analyzed by methods such as time-history diagram, power spectra, and Poincare sections. Studying on it is a meaningful work. Someone interested in the study can read relevant papers such as literatures [27–29]. Improvement of efficiency and accuracy on chatter's prediction by using the different interpolation method in the process of numerical computation is the aim of the paper. So, the prediction error in Fig. 5 is analyzed as follows.

The model of cutting force used in this paper is introduced by Insperger et al. [8] and Bayly et al. [21], and it is a linear model. The above factors such as loss-of-contact effect and process damping are not considered in the cutting force model. As optimization on the process of numerical computation is the aim of the paper, the defect of cutting force model is neglected. Thus, the prediction error in Fig. 5 may be caused by the simplification to the cutting force model. The deficiency of the cutting force model in this paper is the direction for further optimization on the DFDMs proposed above.

5 Conclusions

In this work, the influence of Lagrange interpolation order for the delay term on the regenerative chatter prediction has been studied for the first time, and the 2nd DFDM, 3rd DFDM, 4th

DFDM are proposed. From the research work, the following conclusions are obtained:

1. The higher the order of delay term's Lagrange interpolation is, the more rapidly close the proposed method is to the ideal stability lobe diagram, with the increase of number of time interval m-value, while there is no apparent improvement in time cost;
2. The 4th DFDM has already good prediction accuracy when the m-value is up to 40. Hence, it can be reasonably predicted that hyper-fourth-order DFDM no longer improve the accuracy of stability lobe diagrams apparently.
3. Compared with the updated SDM and 1st FDM, the proposed 2nd DFDM, 3rd DFDM, and 4th DFDM can obviously improve the accuracy and computational efficiency of the regenerative chatter prediction at the same m-value.
4. Compared with 4th FDM at the same m-value, the precision of 4th DFDM is slightly higher. Although it is not apparent which is more rapidly close to the ideal stability lobe diagram between 3rd FDM and 3rd DFDM, the computation time of 3rd DFDM is slightly decreased. It indicates that Lagrange interpolation for delay term of DDEs is more efficient and precise than that for state term. Comparison between 2nd FDM and 2nd DFDM has the same conclusion as comparison between 3rd FDM and 3rd DFDM.
5. When the interpolation order of DFDM rises, the convergence rate of DFDM becomes faster. The influence of interpolation order on the convergence rate can be neglected when the interpolation order reaches to fourth order. Fourth DFDM can be considered as the fastest convergence method in this case. Second DFDM convergence rate is slightly faster than 2nd FDM. Third DFDM's convergence rate is obviously faster than 3rd FDM's.
6. The stability limit gradually increases and the additional form of regenerative chatter is gradually emerging with the decrease of radial immersion ratio. The stability limit of down-milling is slightly lower than that of up-milling. The additional stability lobe diagrams of up-milling and down-milling appear almost at the same speed range and nearly have the same shape, which are affected slightly by the milling method.
7. The results of the theoretical prediction are in good agreement with experimental results by using 4th DFDM. However, it will also show a relatively larger error, in some speed ranges, which may result from the modeling error caused by simplifying the model of cutting force.

Acknowledgments We gratefully acknowledge the financial support for this work from Shenzhen Foundational Research Project (Grant No. 20160427155127098).

Compliance with ethical standards

Conflict of interest The authors declare that they have no conflict of interest.

Appendix

The elements of Eq. (5):

$$\begin{aligned}
\boldsymbol{A}_0 &= \begin{bmatrix} -\xi\omega_{\mathrm{n}} & 1/m_{\mathrm{t}} \\ m_{\mathrm{t}}(\xi\omega_{\mathrm{n}})^2 - m_{\mathrm{t}}{\omega_{\mathrm{n}}}^2 & -\xi\omega_{\mathrm{n}} \end{bmatrix}, \\
\boldsymbol{A}(t) &= \begin{bmatrix} 0 & 0 \\ -wh(t) & 0 \end{bmatrix} \\
\boldsymbol{B}(t) &= \begin{bmatrix} 0 & 0 \\ wh(t) & 0 \end{bmatrix} \\
\boldsymbol{z}(t) &= [x(t)\ \ y(t)]^{\mathrm{T}}
\end{aligned} \tag{32}$$

where

$$y(t) = m_{\mathrm{t}}\dot{x}(t) + m_{\mathrm{t}}\xi\omega_{\mathrm{n}}x(t)\cdot \tag{33}$$

The elements of Eq. (8):

$$\begin{aligned}
\boldsymbol{A}_0 &= \begin{bmatrix} -\boldsymbol{M}^{-1}\boldsymbol{C}/2 & \boldsymbol{M}^{-1} \\ \boldsymbol{C}\boldsymbol{M}^{-1}\boldsymbol{C}/4 - \boldsymbol{K} & -\boldsymbol{C}\boldsymbol{M}^{-1}/2 \end{bmatrix}, \\
\boldsymbol{A}(t) &= \begin{bmatrix} 0 & 0 & 0 & 0 \\ 0 & 0 & 0 & 0 \\ -wh_{\mathrm{xx}}(t) & -wh_{\mathrm{xy}}(t) & 0 & 0 \\ -wh_{\mathrm{yx}}(t) & -wh_{\mathrm{yy}}(t) & 0 & 0 \end{bmatrix}, \\
\boldsymbol{B}(t) &= \begin{bmatrix} 0 & 0 & 0 & 0 \\ 0 & 0 & 0 & 0 \\ wh_{\mathrm{xx}}(t) & wh_{\mathrm{xy}}(t) & 0 & 0 \\ wh_{\mathrm{yx}}(t) & wh_{\mathrm{yy}}(t) & 0 & 0 \end{bmatrix}, \\
\boldsymbol{z}(t) &= [\boldsymbol{q}(t)\ \ \boldsymbol{p}(t)]^{\mathrm{T}},
\end{aligned} \tag{34}$$

where

$$\begin{aligned}
\boldsymbol{p}(t) &= \boldsymbol{M}\dot{\boldsymbol{q}}(t) + \boldsymbol{C}\boldsymbol{q}(t)/2, \\
\boldsymbol{M} &= \begin{bmatrix} m_{\mathrm{t}} & 0 \\ 0 & m_{\mathrm{t}} \end{bmatrix}, \\
\boldsymbol{C} &= \begin{bmatrix} 2m_{\mathrm{t}}\xi\omega_{\mathrm{n}} & 0 \\ 0 & 2m_{\mathrm{t}}\xi\omega_{\mathrm{n}} \end{bmatrix} \\
\boldsymbol{K} &= \begin{bmatrix} m_{\mathrm{t}}{\omega_{\mathrm{n}}}^2 & 0 \\ 0 & m_{\mathrm{t}}{\omega_{\mathrm{n}}}^2 \end{bmatrix}, \\
\boldsymbol{q}(t) &= \begin{bmatrix} x(t) \\ y(t) \end{bmatrix}\cdot
\end{aligned} \tag{35}$$

The elements of Eq. (17):

$$\begin{aligned}
&\boldsymbol{F}_0 = \boldsymbol{\Phi}_0,\\
&\boldsymbol{F}_k = (\boldsymbol{\Phi}_2/\tau)\boldsymbol{A}_0{}^{(k)} + (\boldsymbol{\Phi}_3/\tau)\boldsymbol{A}_1{}^{(k)},\\
&\boldsymbol{F}_{k+1} = (\boldsymbol{\Phi}_1-\boldsymbol{\Phi}_2/\tau)\boldsymbol{A}_0{}^{(k)} + (\boldsymbol{\Phi}_2-\boldsymbol{\Phi}_3/\tau)\boldsymbol{A}_1{}^{(k)},\\
&\boldsymbol{F}_m = \left((\boldsymbol{\Phi}_3 + \tau\boldsymbol{\Phi}_2)/\left(2\tau^2\right)\right)\boldsymbol{B}_0{}^{(k)} + \left((\boldsymbol{\Phi}_4 + \tau\boldsymbol{\Phi}_3)/\left(2\tau^2\right)\right)\boldsymbol{B}_1{}^{(k)},\\
&\boldsymbol{F}_{m+1} = \left(\left(\tau^2\boldsymbol{\Phi}_1-\boldsymbol{\Phi}_3\right)/\left(\tau^2\right)\right)\boldsymbol{B}_0{}^{(k)} + \left(\left(\tau^2\boldsymbol{\Phi}_2-\boldsymbol{\Phi}_4\right)/\left(\tau^2\right)\right)\boldsymbol{B}_1{}^{(k)},\\
&\boldsymbol{F}_{m+2} = \left((\boldsymbol{\Phi}_3-\tau\boldsymbol{\Phi}_2)/\left(2\tau^2\right)\right)\boldsymbol{B}_0{}^{(k)} + \left((\boldsymbol{\Phi}_4-\tau\boldsymbol{\Phi}_3)/\left(2\tau^2\right)\right)\boldsymbol{B}_1{}^{(k)}
\end{aligned} \tag{36}$$

where

$$\begin{aligned}
&\boldsymbol{\Phi}_0 = \mathrm{e}^{\boldsymbol{A}_0\tau},\\
&\boldsymbol{\Phi}_1 = \int_0^\tau \mathrm{e}^{\boldsymbol{A}_0\xi}d\xi = \boldsymbol{A}_0{}^{-1}(\boldsymbol{\Phi}_0-\boldsymbol{I}),\\
&\boldsymbol{\Phi}_2 = \int_0^\tau \xi\mathrm{e}^{\boldsymbol{A}_0\xi}d\xi = \boldsymbol{A}_0{}^{-1}(\tau\boldsymbol{\Phi}_0-\boldsymbol{\Phi}_1),\\
&\boldsymbol{\Phi}_3 = \int_0^\tau \xi^2\mathrm{e}^{\boldsymbol{A}_0\xi}d\xi = \boldsymbol{A}_0{}^{-1}\left(\tau^2\boldsymbol{\Phi}_0-2\boldsymbol{\Phi}_2\right),\\
&\boldsymbol{\Phi}_4 = \int_0^\tau \xi^3\mathrm{e}^{\boldsymbol{A}_0\xi}d\xi = \boldsymbol{A}_0{}^{-1}\left(\tau^3\boldsymbol{\Phi}_0-3\boldsymbol{\Phi}_3\right)\cdot
\end{aligned} \tag{37}$$

The elements of Eq. (25):

$$\begin{aligned}
&\boldsymbol{F}_0=\boldsymbol{\Phi}_0,\\
&\boldsymbol{F}_k = (\boldsymbol{\Phi}_2/\tau)\boldsymbol{A}_0{}^{(k)} + (\boldsymbol{\Phi}_3/\tau)\boldsymbol{A}_1{}^{(k)},\\
&\boldsymbol{F}_{k+1} = (\boldsymbol{\Phi}_1-\boldsymbol{\Phi}_2/\tau)\boldsymbol{A}_0{}^{(k)} + (\boldsymbol{\Phi}_2\text{-}\boldsymbol{\Phi}_3/\tau)\boldsymbol{A}_1{}^{(k)},\\
&\boldsymbol{F}_m = \left(\left(\boldsymbol{\Phi}_4 + 3\tau\boldsymbol{\Phi}_3 + 2\tau^2\boldsymbol{\Phi}_2\right)/\left(6\tau^3\right)\right)\boldsymbol{B}_0{}^{(k)}\\
&\qquad + \left(\left(\boldsymbol{\Phi}_5 + 3\tau\boldsymbol{\Phi}_4 + 2\tau^2\boldsymbol{\Phi}_3\right)/\left(6\tau^3\right)\right)\boldsymbol{B}_1{}^{(k)},\\
&\boldsymbol{F}_{m+1} = \left(\left(-\boldsymbol{\Phi}_4-2\tau\boldsymbol{\Phi}_3+\tau^2\boldsymbol{\Phi}_2 + 2\tau^3\boldsymbol{\Phi}_1\right)/\left(2\tau^3\right)\right)\boldsymbol{B}_0{}^{(k)}\\
&\qquad + \left(\left(-\boldsymbol{\Phi}_5-2\tau\boldsymbol{\Phi}_4+\tau^2\boldsymbol{\Phi}_3 + 2\tau^3\boldsymbol{\Phi}_2\right)/\left(2\tau^3\right)\right)\boldsymbol{B}_1{}^{(k)},\\
&\boldsymbol{F}_{m+2} = \left(\left(\boldsymbol{\Phi}_4 + \tau\boldsymbol{\Phi}_3-2\tau^2\boldsymbol{\Phi}_2\right)/\left(2\tau^3\right)\right)\boldsymbol{B}_0{}^{(k)}\\
&\qquad + \left(\left(\boldsymbol{\Phi}_5 + \tau\boldsymbol{\Phi}_4-2\tau^2\boldsymbol{\Phi}_3\right)/\left(2\tau^3\right)\right)\boldsymbol{B}_1{}^{(k)},\\
&\boldsymbol{F}_{m+3} = \left(\left(-\boldsymbol{\Phi}_4+\tau^2\boldsymbol{\Phi}_2\right)/\left(6\tau^3\right)\right)\boldsymbol{B}_0{}^{(k)}\\
&\qquad + \left(\left(-\boldsymbol{\Phi}_5+\tau^2\boldsymbol{\Phi}_3\right)/\left(6\tau^3\right)\right)\boldsymbol{B}_1{}^{(k)},
\end{aligned} \tag{38}$$

where

$$\begin{aligned}
&\boldsymbol{\Phi}_0 = \mathrm{e}^{\boldsymbol{A}_0\tau},\\
&\boldsymbol{\Phi}_1 = \int_0^\tau \mathrm{e}^{\boldsymbol{A}_0\xi}d\xi = \boldsymbol{A}_0{}^{-1}(\boldsymbol{\Phi}_0-\boldsymbol{I}),\\
&\boldsymbol{\Phi}_2 = \int_0^\tau \xi\mathrm{e}^{\boldsymbol{A}_0\xi}d\xi = \boldsymbol{A}_0{}^{-1}(\tau\boldsymbol{\Phi}_0-\boldsymbol{\Phi}_1),\\
&\boldsymbol{\Phi}_3 = \int_0^\tau \xi^2\mathrm{e}^{\boldsymbol{A}_0\xi}d\xi = \boldsymbol{A}_0{}^{-1}\left(\tau^2\boldsymbol{\Phi}_0-2\boldsymbol{\Phi}_2\right),\\
&\boldsymbol{\Phi}_4 = \int_0^\tau \xi^3\mathrm{e}^{\boldsymbol{A}_0\xi}d\xi = \boldsymbol{A}_0{}^{-1}\left(\tau^3\boldsymbol{\Phi}_0-3\boldsymbol{\Phi}_3\right),\\
&\boldsymbol{\Phi}_5 = \int_0^\tau \xi^4\mathrm{e}^{\boldsymbol{A}_0\xi}d\xi = \boldsymbol{A}_0{}^{-1}\left(\tau^4\boldsymbol{\Phi}_0-4\boldsymbol{\Phi}_4\right).
\end{aligned} \tag{39}$$

The elements of Eq. (29):

$$\begin{aligned}
&\boldsymbol{F}_0 = \boldsymbol{\Phi}_0,\\
&\boldsymbol{F}_k = (\boldsymbol{\Phi}_2/\tau)\boldsymbol{A}_0{}^{(k)} + (\boldsymbol{\Phi}_3/\tau)\boldsymbol{A}_1{}^{(k)},\\
&\boldsymbol{F}_{k+1} = (\boldsymbol{\Phi}_1-\boldsymbol{\Phi}_2/\tau)\boldsymbol{A}_0{}^{(k)} + (\boldsymbol{\Phi}_2\text{-}\boldsymbol{\Phi}_3/\tau)\boldsymbol{A}_1{}^{(k)},\\
&\boldsymbol{F}_m = \left(\left(\boldsymbol{\Phi}_5 + 6\tau\boldsymbol{\Phi}_4 + 11\tau^2\boldsymbol{\Phi}_3 + 6\tau^3\boldsymbol{\Phi}_2\right)/\left(24\tau^4\right)\right)\boldsymbol{B}_0{}^{(k)}\\
&\qquad + \left(\left(\boldsymbol{\Phi}_6 + 6\tau\boldsymbol{\Phi}_5 + 11\tau^2\boldsymbol{\Phi}_4 + 6\tau^3\boldsymbol{\Phi}_3\right)/\left(24\tau^4\right)\right)\boldsymbol{B}_1{}^{(k)}\\
&\boldsymbol{F}_{m+1} = \left(\left(-\boldsymbol{\Phi}_5-5\tau\boldsymbol{\Phi}_4-5\tau^2\boldsymbol{\Phi}_3 + 5\tau^3\boldsymbol{\Phi}_2 + 6\tau^4\boldsymbol{\Phi}_1\right)/\left(6\tau^4\right)\right)\boldsymbol{B}_0{}^{(k)}\\
&\qquad + \left(\left(-\boldsymbol{\Phi}_6-5\tau\boldsymbol{\Phi}_5-5\tau^2\boldsymbol{\Phi}_4 + 5\tau^3\boldsymbol{\Phi}_3 + 6\tau^4\boldsymbol{\Phi}_2\right)/\left(6\tau^4\right)\right)\boldsymbol{B}_1{}^{(k)}\\
&\boldsymbol{F}_{m+2} = \left(\left(\boldsymbol{\Phi}_5 + 4\tau\boldsymbol{\Phi}_4+\tau^2\boldsymbol{\Phi}_3\text{-}6\tau^3\boldsymbol{\Phi}_2\right)/\left(4\tau^4\right)\right)\boldsymbol{B}_0{}^{(k)}\\
&\qquad + \left(\left(\boldsymbol{\Phi}_6 + 4\tau\boldsymbol{\Phi}_5+\tau^2\boldsymbol{\Phi}_4-6\tau^3\boldsymbol{\Phi}_3\right)/\left(4\tau^4\right)\right)\boldsymbol{B}_1{}^{(k)}\\
&\boldsymbol{F}_{m+3} = \left(\left(-\boldsymbol{\Phi}_5-3\tau\boldsymbol{\Phi}_4+\tau^2\boldsymbol{\Phi}_3 + 3\tau^3\boldsymbol{\Phi}_2\right)/\left(6\tau^4\right)\right)\boldsymbol{B}_0{}^{(k)}\\
&\qquad + \left(\left(\text{-}\Phi_6\text{-}3\tau\boldsymbol{\Phi}_5+\tau^2\boldsymbol{\Phi}_4 + 3\tau^3\boldsymbol{\Phi}_3\right)/\left(6\tau^4\right)\right)\boldsymbol{B}_1{}^{(k)}\\
&\boldsymbol{F}_{m+4} = \left(\left(\boldsymbol{\Phi}_5 + 2\tau\boldsymbol{\Phi}_4-\tau^2\boldsymbol{\Phi}_3-2\tau^3\boldsymbol{\Phi}_2\right)/\left(24\tau^4\right)\right)\boldsymbol{B}_0{}^{(k)}\\
&\qquad + \left(\left(\boldsymbol{\Phi}_6 + 2\tau\boldsymbol{\Phi}_5-\tau^2\boldsymbol{\Phi}_4-2\tau^3\boldsymbol{\Phi}_3\right)/\left(24\tau^4\right)\right)\boldsymbol{B}_1{}^{(k)}
\end{aligned} \tag{40}$$

where

$$\begin{aligned}
&\boldsymbol{\Phi}_0 = \mathrm{e}^{\boldsymbol{A}_0\tau},\\
&\boldsymbol{\Phi}_1 = \int_0^\tau \mathrm{e}^{\boldsymbol{A}_0\xi}d\xi = \boldsymbol{A}_0{}^{-1}(\boldsymbol{\Phi}_0-\boldsymbol{I}),\\
&\boldsymbol{\Phi}_2 = \int_0^\tau \xi\mathrm{e}^{\boldsymbol{A}_0\xi}d\xi = \boldsymbol{A}_0{}^{-1}(\tau\boldsymbol{\Phi}_0-\boldsymbol{\Phi}_1),\\
&\boldsymbol{\Phi}_3 = \int_0^\tau \xi^2\mathrm{e}^{\boldsymbol{A}_0\xi}d\xi = \boldsymbol{A}_0{}^{-1}\left(\tau^2\boldsymbol{\Phi}_0-2\boldsymbol{\Phi}_2\right),\\
&\boldsymbol{\Phi}_4 = \int_0^\tau \xi^3\mathrm{e}^{\boldsymbol{A}_0\xi}d\xi = \boldsymbol{A}_0{}^{-1}\left(\tau^3\boldsymbol{\Phi}_0-3\boldsymbol{\Phi}_3\right),\\
&\boldsymbol{\Phi}_5 = \int_0^\tau \xi^4\mathrm{e}^{\boldsymbol{A}_0\xi}d\xi = \boldsymbol{A}_0{}^{-1}\left(\tau^4\boldsymbol{\Phi}_0-4\boldsymbol{\Phi}_4\right),\\
&\boldsymbol{\Phi}_6 = \int_0^\tau \xi^5\mathrm{e}^{\boldsymbol{A}_0\xi}d\xi = \boldsymbol{A}_0{}^{-1}\left(\tau^5\boldsymbol{\Phi}_0-5\boldsymbol{\Phi}_5\right)\cdot
\end{aligned} \tag{41}$$

References

1. Koenigsberger F, Tlusty J (1970) Machine tool structures. Pergamon Press, London
2. Sridhar R, Hohn RE, Long GW (1968) A stability algorithm for the general milling process. ASME J Eng Ind 90(2):330–334. doi:10.1115/1.3604637
3. Altintas Y, Budak E (1995) Analytical prediction of stability lobes in milling. CIRP Ann Manuf Technol 44(1):357–362. doi:10.1016/S0007-8506(07)62342-7
4. Tang WX, Song QH, Yu SQ, Sun SS, Li BB, Du B, Ai X (2009) Prediction of chatter stability in high-speed finishing end milling considering multi-mode dynamics. J Mater Process Technol 209(5):2585–2591. doi:10.1016/j.jmatprotec.2008.06.003
5. Gradišek J, Kalveram M, Insperger T, Weinert K, Stépán G, Govekar E, Grabec I (2005) On stability prediction for milling. Int J Mach Tools Manuf 45(7–8):769–781. doi:10.1016/j.ijmachtools.2004.11.015
6. Budak E, Altintas Y (1998) Analytical prediction of chatter stability in milling—part I: general formulation. J Dyn Syst Meas Control 120(1):22–30. doi:10.1115/1.2801317
7. Insperger T, Stépán G (2002) Semi-discretization method for delayed systems. Int J Numer Methods Eng 55:503–518. doi:10.1002/nme.505
8. Insperger T, Stépán G (2004) Updated semi-discretization method for periodic delay-differential equations with discrete delay. Int J Numer Methods Eng 61:117–141. doi:10.1002/nme.1061
9. Insperger T, Stépán G, Turi J (2008) On the higher-order semi-discretizations for periodic delayed systems. J Sound Vib 313(1–2):334–341. doi:10.1016/j.jsv.2007.11.040
10. Ahmadi K, Ismail F (2012) Modeling chatter in peripheral milling using the semi discretization method. CIRP J Manuf Sci Technol 5(2):77–86. doi:10.1016/j.cirpj.2012.03.001
11. Ding Y, Zhu LM, Zhang XJ, Ding H (2011) Numerical integration method for prediction of milling stability. J Manuf Sci Eng 133. doi:10.1115/1.4004136
12. Liang XG, Yao ZQ, Luo L, Hu J (2013) An improved numerical integration method for predicting milling stability with varying time delay. Int J Adv Manuf Technol 68(9–12):1967–1976. doi:10.1007/s00170-013-4813-4
13. Ding Y, Zhu LM, Zhang XJ, Ding H (2010) A full-discretization method for prediction of milling stability. Int J Mach Tools Manuf 50(5):502–509. doi:10.1016/j.ijmachtools.2010.01.003
14. Ding Y, Zhu LM, Zhang XJ, Ding H (2010) Second-order full-discretization method for milling stability prediction. Int J Mach Tools Manuf 50(10):926–932. doi:10.1016/j.ijmachtools.2010.05.005
15. Quo Q, Sun YW, Jiang Y (2012) On the accurate calculation of milling stability limits using third-order full-discretization method. Int J Mach Tools Manuf 62:61–66. doi:10.1016/j.ijmachtools.2012.05.001
16. Ozoegwu CG, Omenyi SN, Ofochebe SM (2015) Hyper-third order full-discretization methods in milling stability prediction. Int J Mach Tools Manuf 92:1–9. doi:10.1016/j.ijmachtools.2015.02.007
17. Liu YL, Fischer A, Eberhard P, Wu BH (2015) A high-order full-discretization method using Hermite interpolation for periodic time-delayed differential equations. Acta Mech Sinica 31(3):406–415. doi:10.1007/s10409-015-0397-6
18. Tang XW, Peng FY, Yan R, Gong YH, Li YT, Jiang LL (2016) Accurate and efficient prediction of milling stability with updated full-discretization method. Int J Adv Manuf Technol 88(9–12):2357–2368. doi:10.1007/s00170-016-8923-7
19. Li ZQ, Yang ZK, Peng YR, Zhu F, Ming XZ (2015) Prediction of chatter stability for milling process using Runge-Kutta-based complete discretization method. Int J Adv Manuf Technol 86(1–4):943–952. doi:10.1007/s00170-015-8207-7
20. Xie QZ (2015) Milling stability prediction using an improved complete discretization method. Int J Adv Manuf Technol 83(5–8):815–821. doi:10.1007/s00170-015-7626-9
21. Bayly PV, Mann BP, Schmitz TL, Peters DA, Stepan G, Insperger T (2002) Effects of radial immersion and cutting direction on chatter instability in end-milling. Paper presented at the ASME 2002 International Mechanical Engineering Congress and Exposition, New Orleans
22. Kuang J, Cong Y (2005) Stability of numerical methods for delay differential equations. Science Press, Beijing
23. Insperger T (2010) Full-discretization and semi-discretization for milling stability prediction: some comments. Int J Mach Tools Manuf 50(7):658–662. doi:10.1016/j.ijmachtools.2010.03.010
24. Zhao MX, Balachandran B (2001) Dynamics and stability of milling process. Int J Solids Struct 38:2233–2248. doi:10.1016/S0020-7683(00)00164-5
25. Long XH, Balachandran B (2010) Stability of up-milling and down-milling operations with variable spindle speed. J Vib Control 16(7–8):1151–1168. doi:10.1177/1077546309341131
26. Yue C, Liu XL, Liang SY (2016) A model for predicting chatter stability considering contact characteristic between milling cutter and workpiece. Int J Adv Manuf Technol 88(5–8):2345–2354. doi:10.1007/s00170-016-8953-1
27. Balachandran B (2001) Nonlinear dynamics of milling process. Philos Trans R Soc Lond A 359(1781):793–819. doi:10.1098/rsta.2000.0755
28. Balachandran B, Gilsinn D (2005) Non-linear oscillations of milling. Math Comput Model Dyn Syst 11(3):273–290. doi:10.1080/13873950500076479
29. Long XH, Balachandran B (2007) Stability analysis for milling process. Nonlinear Dyn 49(3):349–359. doi:10.1007/s11071-006-9127-8
30. Moradi H, Vossoughi G, Movahhedy MR (2014) Bifurcation analysis of nonlinear milling process with tool wear and process damping: sub-harmonic resonance under regenerative chatter. Int J Mech Sci 85:1–19. doi:10.1016/j.ijmecsci.2014.04.011
31. Tyler CT, Troutman JR, Schmitz TL (2016) A coupled dynamics, multiple degree of freedom process damping model, part 2: milling. Precis Eng 46:73–80. doi:10.1016/j.precisioneng.2016.03.018
32. Wang JJ, Uhlmann E, Oberschmidt D, Sung CF, Perfilov I (2016) Critical depth of cut and asymptotic spindle speed for chatter in micro milling with process damping. CIRP Ann Manuf Technol 65(1):113–116. doi:10.1016/j.cirp.2016.04.088
33. Tyler CT, Troutman J, Schmitz TL (2015) Radial depth of cut stability lobe diagrams with process damping effects. Precis Eng 40:318–324. doi:10.1016/j.precisioneng.2014.11.004
34. Rahnama R, Sajjadi M, Park SS (2009) Chatter suppression in micro end milling with process damping. J Mater Process Technol 209(17):5766–5776. doi:10.1016/j.jmatprotec.2009.06.009
35. Li ZY, Sun YW, Guo DM (2016) Chatter prediction utilizing stability lobes with process damping in finish milling of titanium alloy thin-walled workpiece. Int J Adv Manuf Technol 89(9–12):2663–2674. doi:10.1007/s00170-016-9834-3
36. Budak E, Tunç LT, Alan S, Özgüven HN (2012) Prediction of workpiece dynamics and its effects on chatter stability in milling. CIRP Ann Manuf Technol 61(1):339–342. doi:10.1016/j.cirp.2012.03.144
37. Liu YL, Wu BH, Ma JJ, Zhang DH (2016) Chatter identification of the milling process considering dynamics of the thin-walled workpiece. Int J Adv Manuf Technol 89(5). doi:10.1007/s00170-016-9190-3